Journal of Porous Materials (2019) 26:41–50
https://doi.org/10.1007/s10934-018-0605-4

Synthesis of layered organic–inorganic nanohybrid zinc–aluminium-2-(4-chlorophenoxy)-2-methyl propionic acid with controlled release properties

S. H. Sarijo[1] · A. Ahmad[1] · S. M. N. Muhsin[2] · Z. Jubri[3]

Published online: 26 March 2018

Abstract
A plant growth regulator, 2-(4-chlorophenoxy)-2-methyl propionic acid (CFA), was successfully intercalated into zinc–aluminium layered double hydroxide (ZAL) forming a new nanohybrid composite, zinc–aluminium-2-(4-chlorophenoxy)-2-methylpropionate layered double hydroxide (ZAC). Well-crystallized nanohybrid composite was obtained when the material was synthesized with zinc to aluminium molar ratio, R = 4 and 0.2 M CFA. Due to the intercalation of CFA, basal spacing expanded from 8.9 Å in the ZAL to 21.4 Å in the ZAC. The FTIR spectra of the ZAC nanohybrid composite show resemblance peaks of the ZAL and CFA indicating the inclusion of the organic compound into the LDH interlamellae. The loading percentage of CFA is 40.0% (w/w) calculated based on the percentage of carbon in the sample. The BET surface area increased from 1.0 to 70.0 $m^2\ g^{-1}$ due to the inclusion of CFA into the ZAL interlamellae and associated expansion of the layered structure. Release of CFA from the ZAL interlayer was found to be dependent on the affinity of the incoming anion, in the order of phosphate > sulfate > nitrate with the percentage saturated release of 74, 54, and 42%, respectively. This study indicates the potential application of zinc–aluminium-layered double hydroxide as a host for plant growth regulator, CFA, with controlled release capability.

Keywords 2-(4-Chlorophenoxy)-2-methyl propionic acid · Plant growth regulator · Layered double hydroxide · Nanohybrid composite

1 Introduction

Layered double hydroxides (LDHs) are a class of layered compounds derived from the structure of brucite, which comprises stacks of neutral layers having the composition, $Mg(OH)_2$. Structurally they are formed by brucite-like ($Mg(OH)_2$) sheets where isomorphous substitution of Mg^{2+} by a trivalent cation such as Al^{3+} occurs. When a fraction, x, of Mg^{2+} ions are isomorphously substituted by Al^{3+} ions, the layers acquire the composition $[Mg_{1-x}\ Al_x(OH)_2]^{x+}$, where $0.2 \leq x \leq 0.33$ and become positively charged. The positive charge of the layer is compensated by counter anions, which occupy the interlayer space along with water molecules [1]. Anions such as Cl^-, NO_3^-, CO_3^{2-} are incorporated in the interlayer region along with water molecules to restore charge neutrality and stability [2]. A wide range of such materials can be synthesized directly by co-precipitation or self-assembly [3, 4], anion-exchange [5, 6] and reconstruction method [3, 7]. The interlayer interaction in the LDHs are mediated by coulombic forces between the positively charged layers and the anions in the interlayer and hydrogen bonding between the hydroxyl groups of the layer with the anions and the water molecules in the interlayer [8]. Due to the weak electrostatic interaction between the brucite sheets and the counter anion in the interlayer domain, LDHs has good ion exchange properties and has become a potential adsorbents for the removal of various anions from contaminated water including 2,4-D [9, 10], fulvic and humic acid

✉ S. H. Sarijo
sitihalimah@salam.uitm.edu.my

1 Faculty of Applied Sciences, Universiti Teknologi MARA, 40450 Shah Alam, Selangor, Malaysia

2 Malaysian Palm Oil Board, No. 6, Persiaran Institusi, Bandar Baru Bangi, 43000 Kajang, Selangor, Malaysia

3 Department of Engineering, Sciences and Mathematics, College of Engineering, Universiti Tenaga Nasional, 43000 Kajang, Selangor, Malaysia

[11], chromate [12], arsenite and phosphate [13], to name a few.

More recently intercalation of agrochemicals such as pesticides [14–16] and bactericides [17] into LDHs for controlled release formulations have been investigated. In this case the LDHs interlayer region of the lamellar host act as a microvessel in which the anions can be stored [18] to form organic–inorganic nanohybrids with controlled release property, preventing the problem of volatilization, leaching and degradation, therefore minimizing the risk of the environmental pollution and reducing the amount of chemicals applied for agricultural activities [19]. Agrochemicals such as pesticides are normally applied in large amounts and are easily swept away leading to water pollution problems [20]. The retention of pesticides by soil may prevent its short term access to the surface and groundwater and on nontarget organisms, but the persistence of the undegraded pesticides or of harmful metabolites leads to its accumulation in the environment and increase the risk to human health [21].

2-(4-Chlorophenoxy)-2-methyl propionic acid or so called clofibric acid (Fig. 1) is a plant growth regulator used in agriculture to generate plant growth and development. This work aimed to study the possibility of LDHs as the host carrier for clofibric acid for controlled release agrochemicals. The physicochemical properties of the resulting nanocomposite such as surface area and pore size distribution as well as the release properties of CFA into various aqueous solutions will also be discussed.

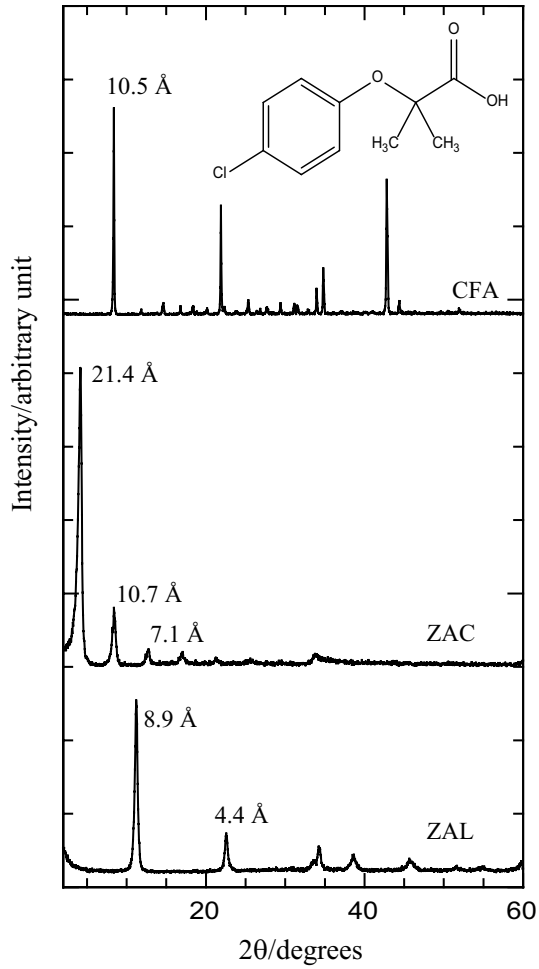

Fig. 1 PXRD patterns of Zn–Al-LDH (ZAL) and the resulting nanocomposites, ZAC synthesized at 0.2 MCFA. The molecular structure of CFA is given in the inset

2 Experimental procedure

All the chemicals used in the synthesis were obtained from various chemical suppliers and used without further purification. $Zn(NO_3)_2 \cdot 6H_2O$ (98%), $Al(NO_3)_3 \cdot 9H_2O$ (98%) and NaOH (97%) were obtained from Merck. 2-(4-Chlorophenoxy)-2-methyl propionic acid (97%) was purchased from Sigma-Aldrich. All solutions were prepared using deionized water. The synthesis of the nanocomposite by intercalation of CFA into ZAL interlayer was done via a self-assembly method. The aqueous solutions of $Zn(NO_3)_2 \cdot 6H_2O$ and $Al(NO_3)_3 \cdot 9H_2O$ were added together to give a mother liquor with a Zn to Al molar ratio of 4. Sodium hydroxide (0.2 M) and 25 ml CFA at various concentrations ranging from 0.025 to 0.6 M was added dropwise to the mother liquor with vigorous stirring under a nitrogen atmosphere at constant pH of 7.5. The slurry formed was aged in an oil bath shaker at 70 °C for 18 h, cooled, centrifuged, washed with deionized water and dried in an oven at 70 °C. The resulting material was ground into fine powder and kept in a sample bottle for further use and characterizations. ZAL was prepared by the same procedure except with addition of CFA.

Powder X-ray diffraction (PXRD) patterns of the samples were recorded between 2° and 60° on a Rigaku Model Ultima IV analytical powder diffractometer unit using Cu-Kα radiation (λ = 1.54 Å) at 40 kV and 20 mA. Fourier transform infrared (FTIR) spectra were recorded using a Perkin-Elmer 1725X Spectrophotometer in the range of 400–4000 cm^{-1}. The elemental composition and Zn/Al molar ratio of the samples were determined using an inductively couple plasma atomic emission spectrometry (ICP-AES) with a Perkin Elmer Spectrophotometer model optima 2000DV under standard condition and CHNS analyzer model CHNS-932 (LECO). Surface morphology of the samples was determined by a field emission scanning electron microscopy (FESEM), Carl Zeiss Supra 40VP model. The BET surface area of the solids was determined using a Micromeritics surface area and pore size analyzer (ASAP 2000) using nitrogen gas adsorption–desorption technique at 77 K together with the BET equation. Thermogravimetric

and differential thermogravimetric analyses (TGA–DTG) were performed using a Mettler Toledo instrument at a heating rate of 10 °C min^{-1} in the range of 35–1000 °C under nitrogen with a flow rate of about 50 ml min^{-1}.

Release of CFA from the ZAC hosts was performed by adding 0.6 mg sample into 3.5 ml 0.0005 M aqueous solutions of Na_3PO_4, Na_2SO_4 and NaCl. The accumulated amount of CFA released into the solution was measured in situ at $\lambda_{max} = 278$ nm, using a Perkin Elmer UV–Vis Spectrophotometer Lambda 35. Data was collected, stored and fitted to zero-, first-and pseudo-second order kinetics model.

3 Results and discussion

Figure 1 shows the PXRD patterns for LDH, ZAL and its nanohybrid composites, ZAC synthesized with a Zn/Al molar ratio of 4 and 0.2 M CFA. ZAC nanocomposite with basal spacing of 21.4 Å was obtained at an optimum concentration of 0.2 M as showed by strong and sharp symmetrical peaks reflecting well-crystallized and ordered layered phase. The ZAL with nitrate as the counter anion in the interlayer shows a typical basal spacing of 8.9 Å, as previously reported [3, 22, 23]. The (003) diffraction peak of ZAC were shifted to a lower 2θ angles than those of ZAL, indicating an expansion of the inorganic layered host. Basal spacing expanded from 8.9 to 21.4 Å confirmed the inclusion of CFA into the ZAL interlayers. In this work, less crystalline materials was formed at lower concentration of CFA (0.025–0.1 M) as shown in Fig. 2 indicated by broad peaks at low 2θ value [24]. Therefore, further characterizations and controlled release studies were conducted on the optimized sample, ZAC prepared with 0.2 M CFA.

Figure 3**a** Illustrates molecular structure and estimated dimensions of energy-minimized CFA. The expected gallery height that could be occupied by CFA moieties was calculated from basal spacing obtained in Fig. 1 by substracting the layer thickness 4.8 Å. Plausible arrangement of CFA moieties are illustrated in Fig. 3b. Bilayer arrangement is proposed with maximized intermolecular π–π interaction between aromatic rings of CFA moieties. Additionally, it is likely that the CFA moieties are arranged in such a way that its methyl groups are turned towards chloride due to intermolecular dipole–dipole interaction between chloride and a hydrogen of the methyl groups, as indicated by dashed lines.

Figure 4 shows the FTIR spectra of ZAL, ZAC and pure CFA. The spectrum of ZAL shows a broad absorbance at 3436 cm^{-1} due to the –OH stretching of hydroxyl group and/or physically adsorbed water molecules. Hydrogen bonding of the interlayer water with guest anions as well as hydroxide groups of the layer lowers the wavenumber compared to the free water vibration [25]. The appearance of a strong band at 1384 cm^{-1} is attributed to the presence of the nitrate anion

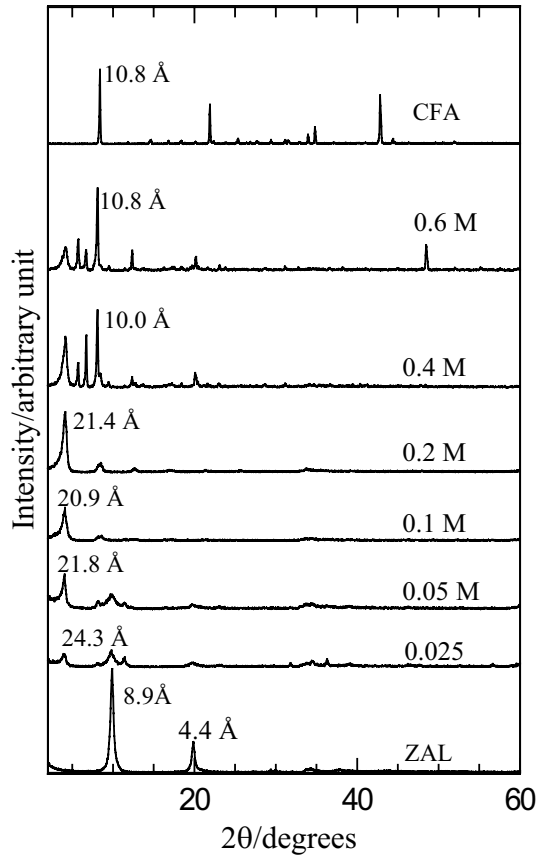

Fig. 2 PXRD patterns of Zn–Al-LDH (ZAL) and the resulting nanocomposites, ZAC synthesized at various concentrations ranging from 0.025 to 0.6 M CFA

in the ZAL interlamellae. A band at 1627 cm^{-1} is due to the H–O–H bending vibration. Bands at 607 and 426 cm^{-1} are due to Al–OH and Zn–Al–OH bending vibrations, respectively [26]. The CFA spectrum exhibits features associated with the carboxylic acid group at 1706 cm^{-1} and OH deformation coupled with C–O stretching vibration at 1231 cm^{-1}. The band observed at 2990 cm^{-1} for CFA is due to the O–H stretching vibration of COOH. The C=C vibrations of the aromatic ring appear at 1489 and 1403 cm^{-1}. Bands at 1305 and 1087 cm^{-1} are due to antisymmetric and symmetric vibration of C–O–C while bands at 1417 and 918 cm^{-1} are due to C–O–H out of plane and in plane bending vibrations, respectively [26]. Bands which appear in the range of 550–730 cm^{-1} are attributed to C–Cl vibrational modes. The ZAC FTIR spectra shows a mixture of CFA and ZAL modes, therefore it is suggested that the intercalation of CFA into the LDH interlayer domain has took place as supported by the PXRD analysis. However due to the intercalation process some of the bands in CFA are slightly shifted to the lower wavelength in ZAC as a result of the interaction between the CFA anion and ZAL. The absence of the absorbance band at 1384 cm^{-1}, as previously present in ZAL spectrum indicates

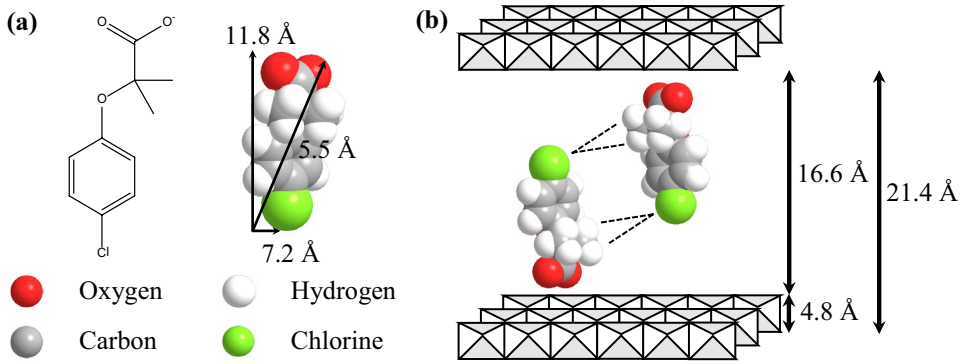

Fig. 3 Molecular structure and three-dimensional molecular model of CFA anion (**a**) and proposed spatial orientation of CFA moieties in Zn/Al-LDH interlayer (**b**)

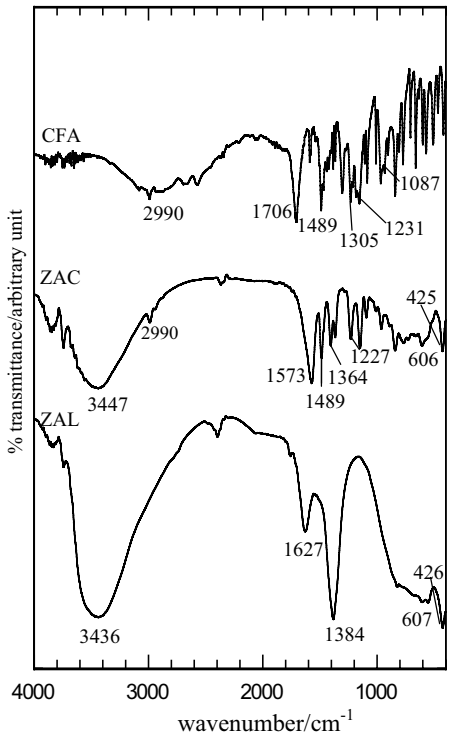

Fig. 4 FTIR spectra of CFA, Zn–Al-LDH (ZAL) and the resulting nanocomposites, ZAC

the absence of nitrate in ZAC. Bands at 1489 and 1409 cm^{-1} are due to the C=C stretching vibration of the aromatic ring. The CFA's C–O–C antisymmetric and symmetric stretching bands appear at 1227 and 1065 cm^{-1}. New bands at 1573 and 1364 cm^{-1} for ZAC is due to the C=O carboxylate anion, indicates the presence of CFA in the anionic form in the interlamellae space of the LDH.

The elemental and organic contents of ZAL and ZAC are shown in Table 1. The molar ratio of Zn to Al in ZAL and ZAC are 3.9 and 3.5, respectively, close to the initial value of 4 in the mother liquor. This indicates that the reaction of the metal salts, $Zn(NO_3)_2{\cdot}6H_2O$ and $Al(NO_3)_3{\cdot}9H_2O$ are essentially completed [27]. The CHNS analysis shows ZAC contained 0% (w/w) nitrogen, consistent with the absence of nitrate absorption band at 1384 cm^{-1} in the ZAC showing all the nitrate ions in the interlamellae were completely replaced by CFA in the sample prepared under optimised conditions. The loading percentage of CFA in the ZAC nanocomposite is 40.0% (w/w) calculated based on the carbon content in the sample. The formulae for the synthesized materials, ZAL and ZAC were calculated based on CHNS, ICP-OES and TGA/DTG results. Based on the data, the proposed formula for ZAL and ZAC are $Zn_{0.81}Al_{0.21}(OH)_2(NO_3^-)_{0.25}{\cdot}0.4H_2O$ and $Zn_{0.77}Al_{0.22}(OH)_2\,(C_{10}H_{11}O_3Cl)_{0.2}\,{\cdot}0.6H_2O$, respectively.

The thermal decomposition curves of CFA, ZAL and ZAC are shown in Fig. 5. Pure CFA shows a temperature maximum at 198.9 °C with a corresponding weight loss of 95.2% due to the decomposition of the organic molecules. ZAL shows two major steps of weight losses at temperature maxima of 6.7 and 25.4% at temperature maxima of 120.7 and 230.1 °C, respectively. The first weight loss corresponds to the removal of both physisorbed water at the surface and between the LDHs interlayer domain and the second stage is due to the simultaneous dehydroxylation and decomposition of intercalated NO_3^-. ZAC exhibits major

Table 1 Basal spacing, chemical composition and surface properties of LDH (ZAL) and zinc–aluminium-2-(4-chlorophenoxy)-2-methylpropionate layered double hydroxide (ZAC)

Sample	d (Å)	Zn/Al ratio	% N (%w/w)	% C (%w/w)	% H (%w/w)	Loading percentage (%w/w)	Surface area ($m^2\,g^{-1}$)	BJH d.p.v. ($cm^3\,g^{-1}$)
ZAL	9.0	3.9	3.6	0.4	2.0	–	1.0	0.0
ZAC	21.4	3.5	0.1	22.3	3.4	40.0	70.0	0.2

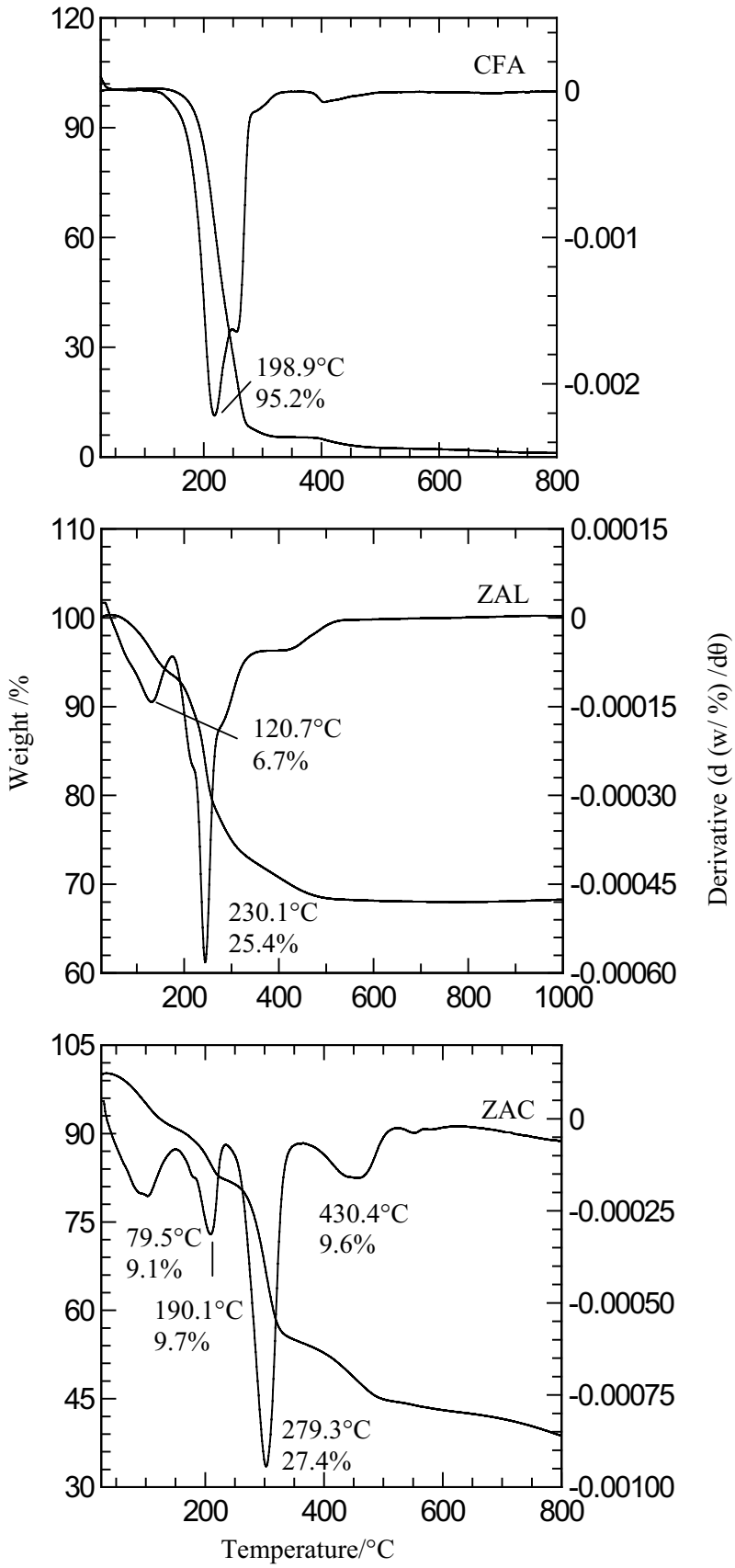

Fig. 5 TGA/DTG thermograms of pure CFA, ZAL and ZAC

thermal decomposition at temperature maxima of 279.3 °C which can be attributed to the intercalated CFA moieties. The higher thermal decomposition temperature indicates that the intercalated anion is thermally more stable in the nanohybrid than in the pure form. Thermal decomposition of ZAC occurs in four steps as shown in Fig. 5. The first stage of weight loss at 79.5 °C is due to the removal of surface physisorbed water amounted of 6.7%. Weight loss of 9.7% at 190.1 °C is attributed to the removal of interlayer anions and dehydroxylation of the hydroxyl layer. Major weight loss amounted of 27.4% is due to the elimination and decomposition of the intercalated organic anion, CFA at 279.3 °C. Simultaneous dehydroxylation and decarbonation of the hydroxide layers occurred at temperature maximum of 430.4 °C with 9.6% weight loss.

The effect of successful intercalation of CFA into Zn–Al-LDH on selected surface properties of the well-ordered hybrid nanocomposite is given in Table 1. The surface area of ZAL synthesized in this work is 1.0 $m^2\ g^{-1}$. The surface area increased to 70.0 $m^2\ g^{-1}$ when CFA was intercalated into the inorganic interlayer of the LDH, replacing the nitrate anion. The intercalation of a bigger anion, CFA, results in the expansion of basal spacing of the resulting nanocomposite and creates more pores and open structures in the crystallites, leading to a significant increase in the surface area. Figure 6a shows the adsorption isotherms for ZAL and ZAC are of type IV with characters indicating the mesoporous nature of the samples. The adsorption branch of the hysteresis loop for ZAF is slightly wider than ZAL, indicating a different pore texture. This can be related to different pore structure when nitrate is replaced by CFA during the formation of ZAC, together with the formation of interstitial pores between the crystallite, and different particle size and morphology. Figure 6b shows the BJH desorption pore size distribution for ZAL and ZAC. As shown in the figure, a broad pore size distribution is observed for both ZAL and ZAC, centered at around 500 Å with the pore volume of the former lower than the latter. The FESEM micrographs in Fig. 7a of ZAL exhibits a flake-like structure with various sizes, ranging from 50 to 400 nm, while ZAC (Fig. 7b) shows an agglomerated granular structure, together with flake-like structure which shows that the inclusion of CFA has changed the structure of ZAL host.

Figure 8 shows the release profile of CFA from the interlamellae of ZAC into phosphate, sulfate and nitrate aqueous solution. The accumulated CFA released into the aqueous solution increased with contact time when ZAC was placed in contact with the aqueous solution. The release rate was found to be fast during the first 50 min followed by a slower release thereafter. The saturated release of CFA was 74, 54, and 42% in PO_4^{3-}, SO_4^{2-}, and NO_3^- aqueous solution, respectively. Equilibrium was achieved at around 350 min for release of CFA in PO_4^{3-}, and SO_4^{2-} aqueous solutions but longer for NO_3^- aqueous solution (around 700 min). The presence of PO_4^{3-}, SO_4^{2-}, and NO_3^- in the aqueous solutions resulted in the ion-exchanged with CFA thus releasing CFA into the aqueous media. At the same time the PO_4^{3-}, SO_4^{2-}, and NO_3^- ions are incorporated into the interlayer domain of ZAL, forming new LDH phases with phosphate, sulfate and nitrate as the counter anion. The ion-exchange process is rapid at the beginning of the experiment and slower thereafter as the equilibrium is approached. When a bigger species, CFA is replaced with smaller anion (PO_4^{3-}, SO_4^{2-}, or NO_3^-), a decrease in basal spacing occurred and this phase transformation will first cover the external part of the nanohybrid crystallites. As the reaction proceeded, a smaller and larger basal spacing co-existed in the same crystal forming a phase boundary between the internal zone containing the nanohybrid and the external zone containing the LDH occurred forming a sort of barrier between ZAC and the aqueous solution, resulting in a decrease in the rate of the CFA released from the nanocomposite into the aqueous solution.

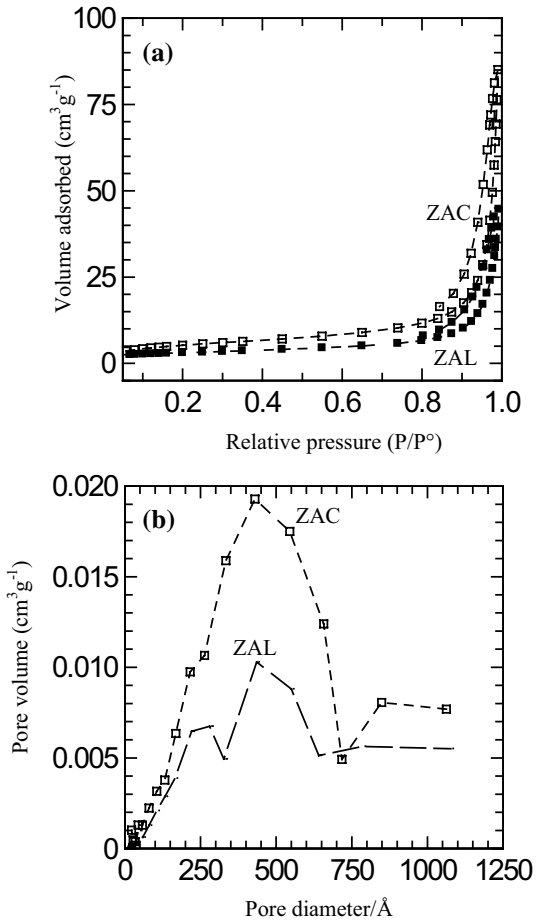

Fig. 6 Nitrogen adsorption–desorption isotherms of ZAL and their nanohybrids, ZAC (**a**) and their pore size distribution (**b**)

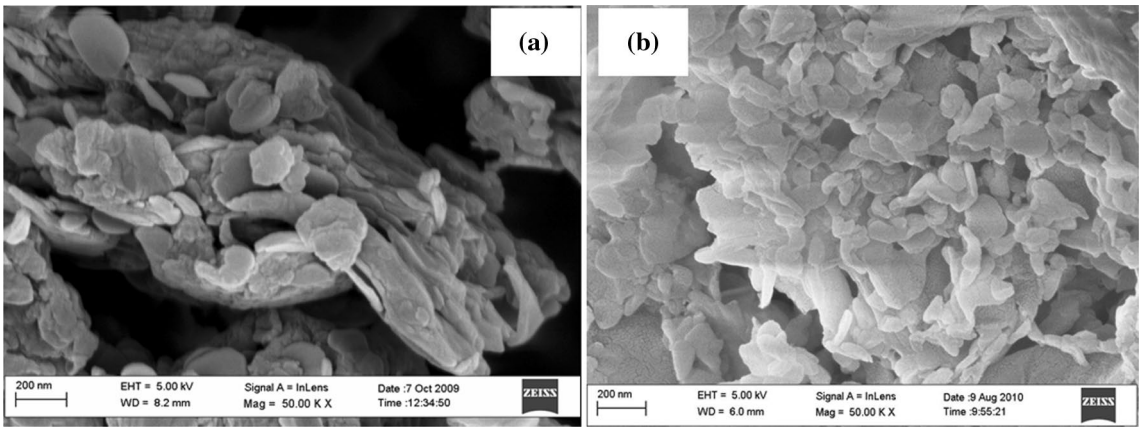

Fig. 7 Surface morphology of ZAL (**a**) and ZAC (**b**) at ×50,000 magnification

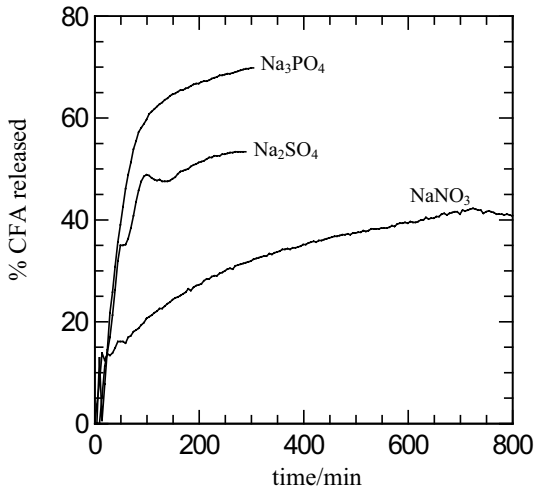

Fig. 8 Release profiles of CFA moieties from the interlamellae of ZAC into aqueous solutions containing 0.0005 M PO_4^{3-}, SO_4^{2-}, and NO_3^- anions

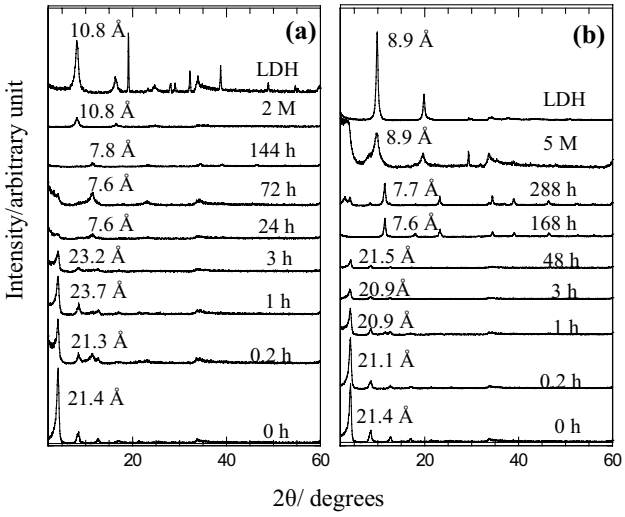

Fig. 9 PXRD patterns of the ZACs recovered from the aqueous solutions containing 0.0005 M sulphate (**a**) and nitrate (**b**) at various release times

This is further evident by the PXRD obtained after stirring the ZAC nanohybrid in 0.0005 M sodium sulfate and sodium nitrate at preset times. The recovered ZAC selected from various contact times were thoroughly washed, dried and characterized by PXRD. As shown in Fig. 9a and b, the LDH-SO_4^{2-} and LDH-NO_3^- were eventually observed after 6 h stirring the ZAC with the 2 M sodium sulfate and 5 M sodium nitrate aqueous solutions, respectively. The PXRD of LDH with sulfate and nitrate as the counter anion were also given at the top of figure for comparison. As shown in the figure, the 003 reflection for ZAC nanohybrids phase reduced in intensity after it was contacted with the aqueous solutions for 1 h contact time.

Due to the anion-exchange of CFA and the anion available in the solution the 'new' LDH phase, which was believed to be Zn–Al-LDH with sulfate and nitrate as the counter anion were formed. These 'new' LDH phases can be clearly observed and the formation of this phase increased as the contact time increased. However the phase changes for ZAC in nitrate medium was very slow and the ZAC phase can still be observed even after 2 days. The LDH-NO_3^- peaks can be observed when the concentration of the sodium nitrate aqueous solution was increased to 5 M. This suggests that the affinity of nitrate towards LDH interlayer is very low compared to sulfate in agreement with results previously described due to lower charge density of nitrate compared to sulfate [3, 4]. The CHNS elemental analysis performed for ZAC recovered from the sodium sulfate aqueous solutions reveals that the sulfur content in ZAC increased while the carbon content decreased at the same time (Fig. 10a). The ZAC recovered from nitrate aqueous solution shows an

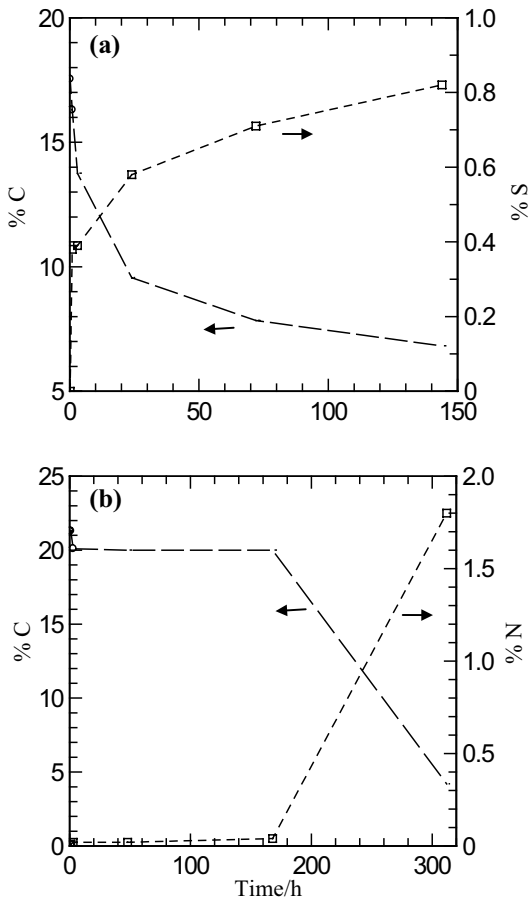

Fig. 10 Plot of percentage of sulphur and carbon (**a**) and carbon and nitrogen (**b**) against time for the samples recovered after the release process of CFA in the aqueous solution containing 0.0005 M sulphate (**a**) and nitrate (**b**) at various release times

increase in the percentage (w/w) of nitrate and a corresponding decrease in carbon percentage (w/w) (Fig. 10b). This shows that CFA in both samples was ion-exchanged and as a result the CFA in the interlamellae is replaced by sulfate and nitrate, forming new LDH-phases.

In order to obtain some insight into the kinetics of release of the phenoxyherbicides anions from their respective nanohybrids, the data obtained from the release study were fitted to zeroth (Eq. 1) [28], first order (Eq. 2) [29] and pseudo second order kinetic models (Eq. 3) [30], as given below, in which C_{eq} and C_t is the percentage release of the herbicides at equilibrium and time, t, respectively, and c is a constant.

$$C_t = kt + c \tag{1}$$

$$-\log(1 - C) = kt + c \tag{2}$$

$$t/C_t = 1/k_2 C_{eq}{}^2 + \left(1/q_e\right) \times t \tag{3}$$

The resulting r^2 values and the parameters obtained from the fitting are listed in Table 2. The plots are given in Fig. 11. The correlation coefficients, r^2 for the linear plots are best fitted by pseudo-second order expression. This suggests that the release of CFA from LDH host can be described by pseudo-second order kinetics, as reflected by the comparison of the r^2 values (Table 2). As a result of the fitting, the $t_{1/2}$ values were calculated to be 41, 40 and 128 min in phosphate, sulfate and nitrate aqueous solution, respectively. The release of CFA into the aqueous solution is in the order of: phosphate > sulfate > nitrate aqueous solution with percentage values of 74, 54, and 42%, respectively. This indicates that CFA is more easily released into the aqueous media if the available anion in the media has higher affinity towards the LDH inorganic interlayers. This shows that the exchangeable anions, either in the release media or in the nanohybrid can be exploited as a means to tune the release properties.

Table 2 Fitting the release of CFA from ZACs into various aqueous solutions of 0.0005 M Na_3PO_4, Na_2SO_4, $NaNO_3$ using zeroth-, first- and pseudo-second order kinetics model for 0–800 min

Media	Zeroth order	First order	Pseudo-second order	k	$t_{1/2}$ (min)
	Regression r^2				
Na_3PO_4	0.673	0.782	0.978	3.0679×10^{-4}	41
Na_2SO_4	0.655	0.726	0.968	4.1644×10^{-4}	40
$NaNO_3$	0.864	0.907	0.989	1.6238×10^{-4}	128

Only k and $t_{1/2}$ for pseudo-second order are given in the table

Zeroth order: $C = kt + c$ [28]

First order $-\log(1-C) = kt + c$ [29]

Pseudo second order $t/C_t = 1/k_2 C_{eq}^2 + \left(1/q_e\right) \times t$ [30]

C_{eq} = concentration of anion at equilibrium, C_o = initial concentration of the anions, C_t = concentration of anion at time t, C = percentage release of anion, c = a constant

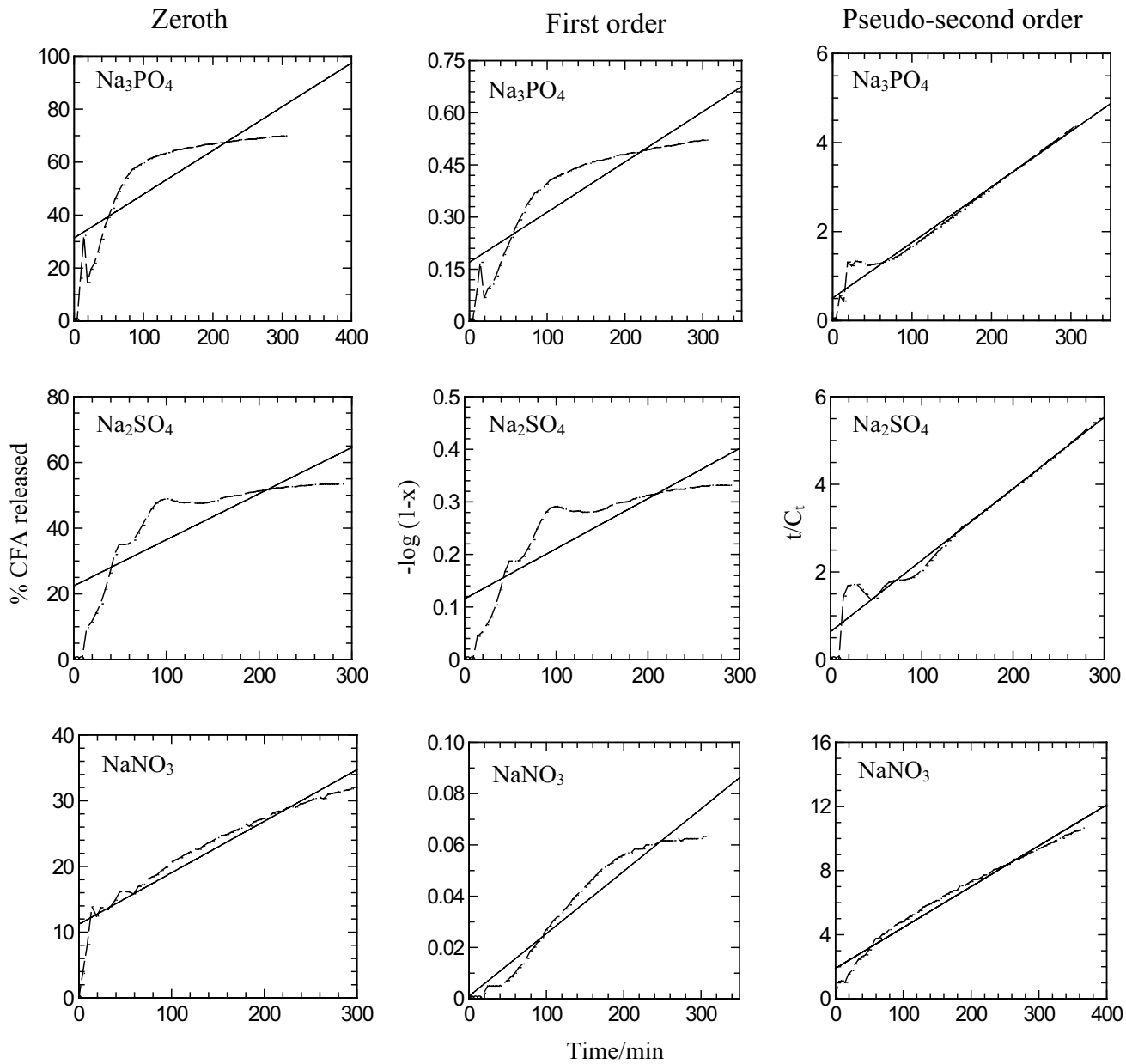

Fig. 11 Fitting the release of CFA from ZACs into various aqueous solutions of 0.0005 M Na_3PO_4, Na_2SO_4, $NaNO_3$ using zeroth-, first- and pseudo-second order kinetics model

4 Conclusion

An organic–inorganic Zn–Al-2-(4-chlorophenoxy)-2-methylpropionate layered double hydroxide nanohybrid was successfully synthesized with the organic moieties, clofibric acid (CFA) interleaved into the Zn–Al-LDH inorganic interlamellae. The release of CFA was found to be dependent on the anions available in the release media which can be expressed by a pseudo-second order rate expression with percentage amount of CFA released in the order of phosphate > sulfate > nitrate. This study suggests that zinc–aluminium-layered double hydroxide is a potential candidate to be used as a host carrier for agrochemical, clofibric acid with controlled release capability.

Acknowledgements Funding for this research was provided by the Ministry of Science, Technology and Innovation of Malaysia (MOSTI), under FRGS Grant No. 600-RMI/ST/FRGS 5/3/FST. A.A. thanks UiTM for the SKS scheme under School of Postgraduate Studies, Faculty of Applied Science.

References

1. J.H. Choy, S.Y. Kwak, Y.S. Han, B.K. Kim, New organo-montmorillonite complexes with hydrophobic and hydrophilic functions. Mater. Lett. **33**, 143 (1997)
2. J.H. Choy, S.Y. Kwak, J.S. Park, Y.J. Jeong, J. Portier, Intercalative nanohybrids of nucleoside monophosphates and DNA in layered metal hydroxide. J. Am. Chem. Soc. **121**, 1399–1400 (1999)
3. S. Miyata, Physicochemical properties of synthetic hydrotalcites in relation to composition. Clays Clay Miner. **28**, 50–56 (1980)
4. V. Rives, *Layered Double Hydroxides: Present and Future* (Nova Scotia Pub Inc, New York, 2001)
5. U. Constantino, N. Coletti, M. Nochetti, Anion exchange of methyl orange into Zn-Al synthetic hydrotalcite and photophysical characterization of the intercalates obtained. Langmuir **15**, 4454–4460 (1999)
6. A.V. Radha, P.V. Kamath, C. Shivakumara, Mechanism of the anion exchange reactions of the layered double hydroxides (LDHs) of Ca and Mg with Al. Solid State Sci. **7**(10), 1180–1187 (2005)
7. H. Nakayama, N. Wada, M. Tsuhako, Intercalation of amino acids and peptides into Mg-Al layered double hydroxide by reconstruction method. Int. J. Pharm. **269**, 469–447 (2004)
8. J.H. Choy, S.Y. Kwak, J.S. Park, Y.J. Jeong, J.S. Park, Inorganic layered double hydroxides as nonviral vectors. Angew. Chem. Int. Ed. **39**, 4041–4045 (2000)
9. A. Chaparadza, J.M. Hossenlopp, Removal of 2,4-dichlorophenoxyacetic acid by calcined Zn-Al-Zr layered double hydroxide. J. Colloid Interface Sci. **363**, 92–97 (2011)
10. Y. Chao, J. Lee, S. Wang, Preferential adsorption of 2,4-dichlorophenoxyacetate from associated binary-solute aqueous systems by Mg/Al-NO_3 layered double hydroxides with different nitrate orientations. J. Hazard Mater. **165**, 846–852 (2009)
11. S. Vreysen, M. Maes, Adsorption mechanism of humic and fulvic acid onto Mg/Al layered double hydroxides. Appl. Clay Sci. **38**, 237–249 (2008)
12. J. Das, D. Das, G.P. Dash, D.P. Das, K. Parida, Studies on Mg/Fe hydrotalcite-like-compound (HTlc):removal of chromium(VI) from aqueous solution. Int. J. Environ. Stud. **61**(5), 605–616 (2004)
13. Y. Xu, Y. Dai, J. Zhou, Z.P. Xu, G. Qian, G.M. Lu, Removal efficiency of arsenate and phosphate from solution using layered double hydroxide materials: intercalation vs. precipitation. J. Mater. Chem. **20**, 4684–4691 (2010)
14. S.H. Sarijo, M.Z. Hussein, N.J. Ghazali, A.I.S.M. Sidek, Synthesis of nanocomposite 2-methyl-4-chlorophenoxyacetic acid with layered double hydroxide: physicochemical characterization and controlled release properties. J. Nanopart. Res. **15**(1), 1356–1364 (2013)
15. F. Bruna, R. Celis, I. Pavlovic, C. Barriga, J. Cornejo, M.A. Ulibarri, Layered double hydroxides as adsorbents and carriers of the herbicide (4-chloro-2-methylphenoxy) acetic acid (MCPA): systems Mg-Al, Mg-Fe and Mg-Al-Fe. J. Hazard. Mater. **168**, 1476–1481 (2009)
16. M.A. Khan, C. Choi, D. Lee, M. Park, B. Lim, J. Lee, J. Choi, Synthesis and properties of mecoprop-intercalated layered double hydroxide. J. Phys. Chem. Solids **68**, 1591–1597 (2007)
17. Q. Zhenlan, Y. Heng, Z. Bin, H. Wanguo, Synthesis and release behavior of bactericides intercalated Mg-Al layered double hydroxides. Colloids Surf. A **348**, 164–169 (2008)
18. Y. El-Nahhal, S. Nir, T. Polubesova, L. Margulies, B. Rubin, Leaching, phytotoxicity, and weed control of new formulations of alachlor. J. Agric. Food Chem. **46**, 3305–3313 (1998)
19. L.P. Cardoso, R. Celis, J. Cornejo, J.B. Valim, Layered double hydroxides as supports for the slow release of acid herbicides. J. Agric. Food Chem. **54**, 5698–5975 (2006)
20. F. Bruna, R. Celis, M. Real, J. Cornejo, Organo/LDH nanocomposite as an adsorbent of polycyclic aromatic hydrocarbons in water and soil–water systems. J. Hazard. Mater. **225–226**, 74–80 (2012)
21. M. Ariaz-Estevez, E. Lopez-Periago, E. Martinez-Carballo, J. Simal-Gandara, J. Mejuto, L. Garcia-Rio, The mobility and degradation of pesticides in soils and the pollution of groundwater resources. Agric. Ecosyst. Environ. **123**, 247–260 (2008)
22. S. Miyata, Anion-exchange properties of hydrotalcite-like compounds. Clays Clay Miner. **31**(4), 305–311 (1983)
23. M.,Z. Barahuie, .Hussein,, P. Arulselvan, S. Fakurazi, Z. Zainal, Drug delivery system for an anticancer agent, chlorogenate-Zn/Al-layered double hydroxide nanohybrid synthesised using direct co-precipitation and ion exchange methods. J. Solid State Chem. **217**, 31–41 (2014)
24. S.P. Newman, W. Jones, Synthesis, characterization and applications of layered double hydroxides containing organic guests. New J. Chem. **22**, 105–115 (1998)
25. D.L. Pavia, G.M. Lampman, G.S. Kriz, J.R. Vyvyan, *Introduction to Spectroscopy*, 4th edn. (USA Brooks/Cole Cengage Learning, Belmont, 2009)
26. A.M. Bashi, M.Z. Hussein, Z. Zainal, M. Rahmani, D. Tichit, Simultaneous intercalation and release of 2,4-dichloro- and 4-chloro-phenoxy acetates into Zn/Al layered double hydroxide. Arab. J. Chem. **9**, S1457–S1463 (2016)
27. M. Badreddine, A. Legrouri, A. Barroug, J.P. Besse, Ion exchange of different phosphate ions into the zinc-aluminium-chloride layered double hydroxide. Mater. Lett. **38**(6), 391–395 (1999)
28. J.W. Hill, R.H. Petrucci, in *General Chemistry. An Integrated Approach*, 3rd edn. (Prentice Hall, Hardcover, 2002)
29. H. Zhang, K. Zou, S. Guo, X. Duan, Nanostructural drug-inorganic clay composites: structure, thermal property and in vitro release of captopril-intercalated Mg-Al-layered double hydroxides. J. Solid State Chem. **179**, 1792–1801 (2006)
30. Y.S. Ho, G. McKay, Pseudo-second order model for sorption processes. Process Biochem. **34**, 451–465 (1999)